Electric manipulation of the Mn-acceptor binding energy and the Mn-Mn exchange interaction on the GaAs (110) surface by nearby As vacancies

M. R. Mahani,[1] A. H. MacDonald,[2] and C. M. Canali[1]
[1]*Department of Physics and Electrical engineering, Linnaeus University, 391 82 Kalmar, Sweden*
[2]*Department of Physics, University of Texas at Austin, Austin, Texas 78712, USA*
(Received 12 December 2014; published 14 July 2015)

We investigate theoretically the effect of nearby As (arsenic) vacancies on the magnetic properties of substitutional Mn (manganese) impurities on the GaAs (110) surface, using a microscopic tight-binding model which captures the salient features of the electronic structure of both types of defects in GaAs. The calculations show that the binding energy of the Mn acceptor is essentially unaffected by the presence of a neutral As vacancy, even at the shortest possible V_{As}-Mn separation. On the other hand, in contrast to a simple tip-induced-band-bending theory and in agreement with experiment, for a positively charged As vacancy the Mn-acceptor binding energy is significantly reduced as the As vacancy is brought closer to the Mn impurity. For two Mn impurities aligned ferromagnetically, we find that nearby charged As vacancies enhance the energy level splitting of the associated coupled acceptor levels, leading to an increase of the effective exchange interaction. Neutral vacancies leave the exchange splitting unchanged. Since it is experimentally possible to switch reversibly between the two charge states of the vacancy, such a local electric manipulation of the magnetic dopants could result in an efficient real-time control of their exchange interaction.

DOI: 10.1103/PhysRevB.92.045304 PACS number(s): 75.50.Pp, 71.55.−i

I. INTRODUCTION

State-of-the-art scanning tunneling microscopy (STM) is nowadays able to manipulate and probe the physical properties of individual impurities located near the surface of a semiconductor. Scanning tunneling spectroscopy (STS) along with STM provides excellent spatial and energy resolution down to the atomic scale. These techniques have been used to study the magnetic and electronic properties of individual Mn impurities in GaAs [1,2] and visualize the topography of the acceptor state bound to Mn on the GaAs (110) surface [3,4]. A more recent advance of these techniques employs the electric field generated by an As vacancy in GaAs to influence the environment surrounding substitutional Mn impurities in the host material [5]. By using STM, it is possible to place As vacancies in GaAs with atomic precision, switch the vacancy between its charge states, and address the effect of the As vacancy electrostatic field on individual Mn acceptors.

The electronic structure and charge state of As vacancies in GaAs have been investigated theoretically and experimentally over the past two decades [6–17]. The most stable charge state of As vacancies has been the topic of a long debate. For dopants in bulk GaAs, the *ab initio* work in Refs. [7,8] showed that the (+3) charge state in *p*-type GaAs is the most stable charge state of an As vacancy, while this value is (+1) for *n*-type GaAs. This result was confirmed later by tight-binding calculations [10]. Determining the stable charge state of an As vacancy on the (110) surface of GaAs turned out to be more challenging and, for a while, contradictory conclusions were reached. STM experiments along with tight-binding calculations [14] show that (+2) is the stable charge state of an As vacancy on the *p*-type GaAs (110) surface, while a pseudopotential calculation [16] found a charge state (−1) instead. However, a more careful *ab initio* study of As vacancies on the GaAs (110) surface [6] suggested (+1) as the stable charge state. Further support for the (+1) charge state as the most stable state of As vacancies on the *p*-type GaAs (110) surface was provided later by *ab initio* work [9,15,17] and by recent STM experiments [5]. Based on this evidence, among the possible charged states of the As vacancies in GaAs, in this paper we consider the (+1) state, together with the neutral state.

In addition to the charge state, the electronic structure of As vacancies has also been investigated [9,15]. Kim and Chelikowsky [9] studied the electronic structure of As vacancies on the GaAs (110) surface using *ab initio* methods. Their calculations show the presence of three distinct doubly degenerate vacancy levels, one of which is fully occupied and lies in the valence band, while the other two levels are within the GaAs band gap. The occupancy of these two levels depends on the charge state of the As vacancy: For a neutral vacancy, the lowest of the two is half filled, while the other is empty. For a (+1) charge state, both levels are empty. The double degeneracy of these levels, which is a trivial spin degeneracy if spin-orbit interaction is neglected, is preserved in the presence of spin orbit as a Kramer's degeneracy as a consequence of time-reversal symmetry. In a second publication [15] the same authors provided a more thorough analysis of the single-particle energy levels of substitutional As vacancies placed on a *p*-type GaAs (110) surface, together with theoretical STM topographies of As vacancies.

Before reviewing the experimental work on the effect of As vacancies on the Mn-acceptor states in GaAs [5], we would like to mention relevant studies on Mn near the GaAs (110) surface. Mn dopants in GaAs have been extensively studied theoretically by first-principles calculations [18–21] and microscopic tight-binding (TB) models [22–30], as well as experimentally by STM techniques [1–3,31,32]. Among theoretical studies, TB models are computationally efficient, which is valuable for studies of impurity problems because of the necessity of large supercell sizes. They have been particularly successful in describing the complex electronic and magnetic properties of

some TM impurities, such as Mn dopants, and their associated acceptor states [22,23,25,26,28,30,33]. In the case of a pair of Mn, TB calculations [3,27,34] have provided insight into the magnetic interactions between substitutional Mn ions near the surface of GaAs. The high-resolution STM measurements in Refs. [3,4], studied a pair of ferromagnetically coupled Mn atoms on the GaAs surface, demonstrating [3,27,34] that the splitting between the two acceptor levels measured by STM is related to the exchange interaction between the Mn atoms.

Control over the acceptor binding energy of a substitutional Mn dopant in GaAs by charged vacancies was recently studied in Ref. [5]. The authors were able to use a STM tip to place As vacancies in the vicinity of Mn dopants, and switch reversibly the charge state of the As vacancy [from a (+1) state to a neutral state] by applying a small voltage pulse. Although a neutral vacancy did not change the binding energy of the Mn acceptor, a positively charged vacancy was found to decrease the Mn-acceptor binding energy by an amount that increases with decreasing As-vacancy–Mn-dopant separation.

In this paper we provide a theoretical simulation of neutral and charged As vacancies, providing the electronic properties of As vacancies in agreement with previous studies. The effects of As vacancies on the Mn-acceptor binding energy have been calculated theoretically, and the results are compared with recent experiment. In addition to one Mn impurity, our calculations predict the enhancement of the acceptor splitting between a pair of ferromagnetically coupled Mn on a GaAs (110) surface.

The paper is divided into the following sections. In Sec. II, we introduce a theoretical approach to model substitutional Mn impurities in the presence of neutral and charged As vacancies on a GaAs (110) surface, extending the TB model for Mn impurities in GaAs originally introduced in Ref. [26]. In Sec. III A, we present results for the electronic properties of an As vacancy on a GaAs (110) surface. Among all the possible charged states of As vacancies on GaAs (110) surfaces, we consider only the +1 state, V_{As}^{+}, which is the most stable in p-doped samples, together with the neutral state, V_{As}^{0}. In the Sec. III B we use the theoretical model to investigate the effect of V_{As}^{0} and V_{As}^{+} on the properties of an individual substitutional Mn. We focus on the physical mechanism leading to the reduction of the Mn-acceptor binding energy caused by nearby charged As vacancies. In Sec. III C we investigate the effect of As vacancies on the exchange interaction between two ferromagnetically coupled Mn dopants on the GaAs (110) surface. Based on the results of our calculations, we predict that the energy splitting between two coupled Mn-acceptor states should increase under the electrostatic potential of a nearby positively charged vacancy. This prediction should be experimentally verifiable. Our calculations also reveal that nearby As vacancies introduce unoccupied midgap impurity levels in addition to those the ones associated with the Mn acceptor only. These extra states are coupled in a nontrivial way with the Mn states and should also be visible as additional peaks in STM measurements. Finally, in Sec. IV, we present our conclusions and we discuss the possibility of using vacancy-induced local electric fields to manipulate the quantum exchange interaction between pairs of magnetic dopants.

II. THEORETICAL MODEL

In this section we review the theoretical TB model introduced in Ref. [26] to describe substitutional Mn impurities in GaAs and complement it with an additional new term modeling neutral (V_{As}^{0}) or positively charged (V_{As}^{+}) As vacancies.

The total TB Hamiltonian is

$$H = H_{\mathrm{MnGaAs}} + H_{V_{As}^{0/+}}. \tag{1}$$

The Hamiltonian for Mn dopants in a GaAs host crystal, H_{MnGaAs}, is

$$\begin{aligned} H_{\mathrm{MnGaAs}} = & \sum_{ij,\mu\mu',\sigma} t^{ij}_{\mu\mu'} a^{\dagger}_{i\mu\sigma} a_{j\mu'\sigma} + J_{pd} \sum_{m} \sum_{n[m]} \vec{S}_n \cdot \hat{\Omega}_m \\ & + \sum_{i,\mu\mu',\sigma\sigma'} \lambda_i \langle \mu,\sigma | \vec{L} \cdot \vec{S} | \mu',\sigma' \rangle a^{\dagger}_{i\mu\sigma} a_{i\mu'\sigma'} \\ & + \frac{e^2}{4\pi\varepsilon_0\varepsilon_r} \sum_{m} \sum_{i\mu\sigma} \frac{a^{\dagger}_{i\mu\sigma} a_{i\mu\sigma}}{|\vec{r}_i - \vec{R}_m|} + V_{\mathrm{corr}}. \end{aligned} \tag{2}$$

Here i and j are atomic indices for Ga and As atoms, m runs over Mn atoms, and $n[m]$ is an index labeling the As atoms that are nearest neighbors of the Mn dopants. The orbital indices μ, ν describe a sp^3 model; σ is the spin index. The first term in Eq. (2) contains the near-neighbor Slater-Koster TB parameters [35,36]. For surface calculations, we rescale the parameters to account for surface relaxation [26,37,38].

The second term implements the antiferromagnetic exchange coupling between the Mn spin, $\hat{\Omega}_m$, treated as a classical vector, and the quantum spin of the nearest-neighbor As p orbitals ($\vec{S}_n = 1/2 \sum_{\pi\sigma\sigma'} a^{\dagger}_{n\pi\sigma} \vec{\tau}_{\sigma\sigma'} a_{n\pi\sigma'}$). Our sp^3 TB Hamiltonian does not explicitly include Mn d orbitals. We use instead this effective exchange interaction term to capture the effect of the hybridization between Mn d orbitals and the nearest-neighbor As p orbitals. The choice of the exchange coupling constant ($J_{pd} = 1.5$ eV) has been inferred from theory [24] and experiment [39]. In a recent publication [33], we have shown that for Mn impurities the classical spin model (the model used in this paper) and the d-level model (the model which includes the d orbitals of Mn explicitly) give the same results. However, the computational needs for the two models are not the same. Our motivation for choosing the classical spin model over the d level model was to increase the computational feasibility for the As vacancy problem addressed here. The merits and limitations of this effective model have been discussed in detail in Ref. [33].

The next term is the spin-orbit interaction with the spin-orbit splitting parameters taken from Ref. [40]. The interplay between the spin-orbit coupling and exchange interaction is the origin of the dependence of the acceptor wave function and level spectra on the direction of the Mn magnetic moment ($\hat{\Omega}_m$) [22,23,26,30,33].

The fourth term is a long-range repulsive Coulomb potential which captures the electrostatic potential produced by the Mn ion. This potential tends to repel electrons and prevents extra electrons from approaching the impurity atom and, therefore, prevents it from charging. This long-range potential is dielectrically screened by the host. The screening constant on the surface is reduced approximately by a factor of two with respect to the bulk value $\varepsilon_r = 12$. This crude representation of

the reduced screening at the surface is qualitatively supported by experimental results [41].

The last term $V_{\rm corr}$ consists of two parts: an on-site potential influencing the Mn ion and an off-site term one affecting its nearest neighbors. The correction term for the Mn is estimated to be ≈1.0 eV from the ionization energy of Mn. We choose the value of the nearest-neighbor off-site potential by tuning the position of the acceptor level to be at the experimentally observed position [42–45]. The acceptor lies at 113 meV above the valance band for Mn in the bulk and ≈850 meV above the valence band for Mn on the surface. This model successfully reproduces most of the electronic and magnetic properties of Mn in GaAs [26].

The second term in Eq. (1) is a one-body effective potential describing the As vacancy. In order to model a neutral As vacancy, V^0_{As}, we add a large positive on-site energy on the As site where the vacancy resides. This large on-site energy gives rise to V^0_{As} impurity states in the gap. In the case of a charged vacancy, V^+_{As}, we introduce the additional term

$$H_{V^+_{As}} = -\frac{e^2}{4\pi\varepsilon_0\varepsilon_r}\sum_{i\mu\sigma}\frac{a^\dagger_{i\mu\sigma}a_{i\mu\sigma}}{|\vec{r}_i-\vec{r}_{\rm vac}|}. \quad (3)$$

Equation (3) represents an attractive potential for electrons and is only added to the Hamiltonian when the charge state of vacancy is positive. It is, in fact, a long-range potential for a positive point charge, dielectrically screened by the host in a way similar to the procedure explained above for the Mn ion, which gives rise to the V^+_{As} impurity states in the gap.

The electronic and magnetic properties of a single substitutional Mn atom in the presence of an As vacancy are obtained by performing supercell-type calculations on finite clusters. Based on our computational resources, typically we are able to fully diagonalize and obtain the entire eigenvalue spectrum of the one-particle Hamiltonian in Eq. (1) for clusters with up to 3200 atoms. For surface calculations we apply periodic boundary conditions in the two (110) surface plane directions. This corresponds to a 38×38 A^2 surface and a supercell cluster that has 20 atomic layers along the surface normal separating the two (110) surfaces [26].

In order to reach large-enough separations between the Mn impurities and the As vacancies on the surface and model the experimental situation, larger clusters with larger surface areas are needed. In this case it is not feasible to fully diagonalize the Hamiltonian. Therefore, for clusters larger than 3200 atoms, we used instead the Lanczos method, which allowed us to compute eigenvalues in an energy window of interest [46], typically one centered inside the gap of the host material, where the important impurity levels are located. With this method we were able to consider clusters containing up to 8840 atoms, whose dimensions in terms of atomic layers are $20 \times 34 \times 52$ along $[110] \times [1\bar{1}0] \times [001]$ crystalline directions. These clusters were large enough to allow us to simulate As-vacancy–Mn-impurity separations of the order of 4 nm. The outputs of the two methods (full diagonalizations vs Lanczos) were systematically compared for clusters up to 3200 atoms to ensure the reliability of the Lanczos diagonalization procedure. We relaxed the position of atoms on the (110) surface layer following a procedure introduced in Refs. [37,38] to remove artificial dangling-bond states.

We would like to point out that there might be some distortions around the As vacancy not considered in the present calculations. However, we believe that the relaxation around the As vacancy would essentially lead to a further small tuning of the electronic energy levels, as the level structure of vacancy in both neutral and positively charged cases in our calculations agrees reasonably well with previous first-principles calculations. In any case, since the distortions around the As vacancy might be more significant than analogous distortions around the Mn, a more thorough analysis of this issue is warranted in future studies.

III. RESULTS AND DISCUSSION

This section is divided into three parts. We discuss the electronic properties of individual As vacancies on the GaAs (110) surface in their neutral and positive charge states in Sec. III A. In Sec. III B, we explain the effects of an As vacancy, in two different charge states, on the electronic properties of one Mn impurity on the GaAs (110) surface. Finally, in Sec. III C, we analyze the electronic and magnetic properties of a pair of ferromagnetically coupled Mn impurities in the presence of an As vacancy.

A. Individual As vacancies on the GaAs (110) surface

Before investigating the effects of As vacancies on the electronic and magnetic properties of nearby Mn impurities on the GaAs (110) surface, we discuss the electronic properties of the As vacancies alone. The +1 state, V^+_{As}, is believed to be the most stable charge state of an As vacancy on a p-type GaAs (110) surface [5,6,9,17]. Therefore, throughout the paper, we only present results for V^+_{As} and the neutral state V^0_{As}. It is possible to switch reversibly between these two charge states using an STM tip [5].

Figure 1(c) shows the level structure of V^0_{As} and V^+_{As} inside the GaAs gap. According to Fig. 1(c), a V^0_{As} defect introduces two doubly degenerate impurity levels in the gap. [It is important to point out that in our finite-cluster calculations for a pure GaAs cluster, that is, without As vacancies, there are no levels in the gap. Therefore, the levels plotted in Fig. 1(c) are directly due to the presence of the As vacancy.] The energies of these levels are respectively at 0.63 eV (half filled) and 0.9 eV (unoccupied) above the top of the valence band. The position, degeneracy, and occupancy of these levels are consistent with previous work based on first-principles calculations [15], in which these two levels are reported to be at 0.67 and 0.82 eV, respectively.

In our calculations the occupancy of these single-particle levels in the many-body ground-state single Slater determinant is determined simply by filling all electronic energies obtained by diagonalizing the Hamiltonian, starting from the lowest levels, with the valence electrons available in the finite cluster. The electron number is given by

$$N_e = 3 \times N_{\rm Ga} + 5 \times N_{\rm As}. \quad (4)$$

For example, in a GaAs cluster of 8840 atoms with one As vacancy, the number of Ga atoms is 4420 and the number of As atoms is $(4420 - 1)$, leading to 35 355 valence electrons in the cluster. (For a pure GaAs cluster in the absence of the

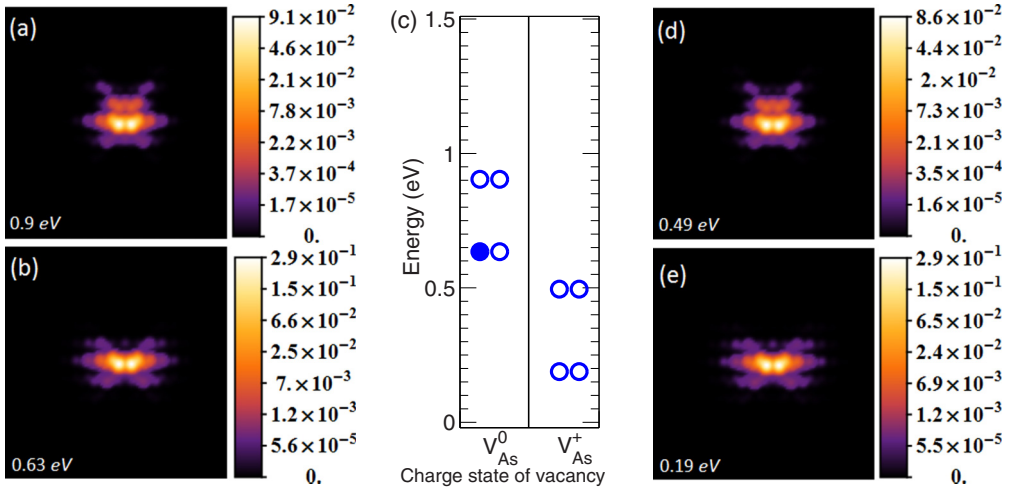

FIG. 1. (Color online) The level structure (c) and the local density of states (LDOS) [(a),(b) and (d),(e)] for an individual As vacancy on the GaAs (110) surface. (a),(b) LDOS of the two V^0_{As} bound impurity levels in panel (c). The impurity levels are identified in (a) and (b) by their energies plotted on the left-hand side of panel (c). (c) The impurity structure for two different charge states of an As vacancy inside the GaAs gap. The zero of energy corresponds to the valence band maximum of GaAs. V^0_{As} stands for neutral and V^+_{As} for positively charged As vacancies. (d),(e) LDOS of the two V^+_{As} impurity levels in panel (c). The orbitals in (d) and (e) are identified by their energies plotted on the right-hand side of panel (c). In each case the LDOS of the two orbitals in the degenerate pairs are identical.

vacancy, this simple counting correctly reproduces, within a discrete particle-level picture, the separation between occupied valence band states and empty conduction band states.)

Figures 1(a) and 1(b) show the local density of states (LDOS) for the two V^0_{As} levels of Fig 1(c). Note that the LDOS is plotted for the wave function of one of each doubly degenerate level due to the similarity of the two. The LDOS shows that the twofold degenerate level at 0.63 eV is mainly localized on the two Ga atoms neighboring the As vacancy. In fact, 29% of the spectral weight is located on each neighboring Ga site. On the other hand, the LDOS for the level at higher energy (0.9 eV) shows less concentration of the spectral weight (only around 10%) on the two neighboring Ga atoms.

By changing the charge state of the vacancy from V^0_{As} to V^+_{As}, the energies of the levels inside the gap change, as illustrated in Fig. 1(c). In V^+_{As}, the two doubly degenerate levels in the gap are pushed closer to the valance band than in the V^0_{As} case. Their positions are at 0.19 and 0.49 eV. The level corresponding to the half-filled level in V^0_{As} is now unoccupied; indeed, the simple electron counting of Eq. (4) gives one fewer electron because the vacancy has one positive charge. These levels correspond to two levels at 0.27 and 0.43 eV, reported previously [15] for V^+_{As}. In spite of the energy shifts, the LDOS for these two levels, illustrated in Figs. 1(d) and 1(e), resemble those of V^0_{As} case. Before closing this section we should mention that both V^0_{As} and V^+_{As} have resonances in the valance band that lie at -0.36 and -0.68 eV, respectively. These two energy values are close to ones previously reported in Ref. [15], -0.32 and -0.66 eV. The LDOSs at these energies is plotted in Fig. 2. Although the shape of the LDOS around the vacancy site is similar to the one of the in-gap states discussed above, the eigenfunctions are considerably delocalized, as expected. We do not address these valance states in the rest of the paper; instead, we focus on the level structure inside the GaAs gap.

B. One Mn impurity with nearby As vacancies

We now consider the effects of V^0_{As} and V^+_{As} on the electronic properties of individual Mn dopants. In the absence of As vacancies, a substitutional Mn atom (replacing a Ga atom) on the GaAs (110) surface introduces three levels in the GaAs gap. These three levels are shown in Fig. 3(a) (red circles). The highest level in energy is unoccupied (empty red circle) and, according to estimates based on STM experiments [3,5], is a deep level that lies at $\approx$0.85 eV above the valence-band edge (energy = 0). We refer to this level as the *Mn acceptor*. The electronic and magnetic properties of the Mn acceptor on the GaAs (110) surface have been studied extensively in the past 8 yr [3,5,25,26,30,33,41]. The model described by Eq. (2) reproduces essentially all the features seen in STM experiments.

In Fig. 3 we plot the electronic structure inside the GaAs gap for the V^0_{As}–Mn-impurity system for several different impurity-vacancy separations. In Fig. 3(a) we superimpose the Mn-impurity states, calculated in the absence of any vacancy, onto the V^0_{As} states, calculated in the absence of the Mn impurity. Blue color indicates states localized near the vacancy and red color indicates a state localized near the Mn, while solid and open circles distinguish states that are occupied and

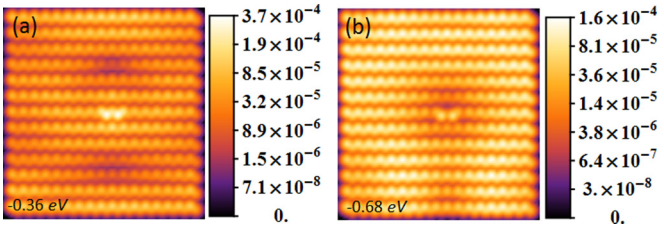

FIG. 2. (Color online) LDOS of As vacancy resonances in the valance band. (a) LDOS for a neutral As vacancy level at -0.36 eV; (b) LDOS for a positively charged vacancy at -0.68 eV.

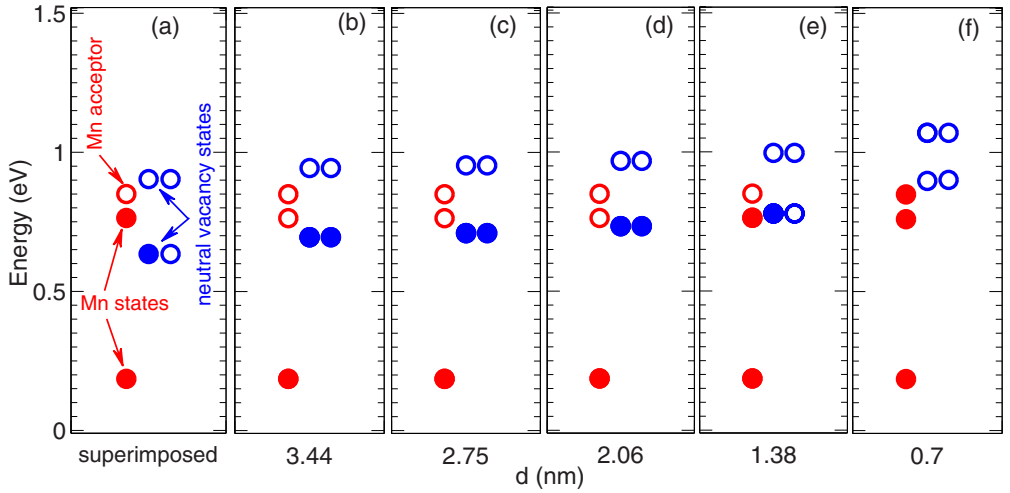

FIG. 3. (Color online) The level structure of the Mn-impurity–neutral-As-vacancy defect complex on the GaAs (110) surface for several different Mn-V^0_{As} separations. (a) The superimposed level spectrum for decoupled Mn and neutral As vacancy defects. (b)–(f) The level structure inside the GaAs gap for different impurity-vacancy separations is shown on the bottom of each panel. The blue circles indicate vacancy states and the red circles Mn states. Solid and open circles are occupied and empty states, respectively.

empty, respectively, in an independent electron approximation. This panel is used as a reference case to compare the electronic structures of the Mn impurity and the As vacancy at different impurity-vacancy separations. Note that in Fig. 3(a), which describes the case of large impurity-vacancy separations, the highest occupied Mn level is higher in energy than the lowest unoccupied V^0_{As}) orbital. Figures 3(b)–3(f) show how the Mn impurity and As vacancy states are perturbed at various finite distances from one another. As the distance between Mn impurity and As vacancy decreases, the V^0_{As} states are slightly pushed up toward the conduction band, while the Mn states, and more specifically the Mn acceptor, defined as the Mn highest unoccupied level in Fig. 3(a), remain unshifted.

In our model the reason for the increase of the vacancy energy levels is the presence of the one-body potential in Eq. (2), coming from the Mn ion. This potential is positive and repels electrons from the Mn core, and it has the effect of raising also the single-particle energy levels introduced by the presence of the vacancy. At larger separations, the long-range contribution of this potential [last but one term in Eq. (2)] is mainly responsible for this effect, as one can evince from the slow increase of the vacancy levels with decreasing distance d. However, in close proximity to the Mn impurity [Fig. 3(f)], short-range contributions coming from V_{corr} can indirectly affect the vacancy levels and cause a more pronounced increase of the energy levels at the shortest separation $d = 0.7$ nm.

In an independent electron approximation, the variation of the energy levels of V^0_{As} with respect to the Mn levels causes the occupancy of both V^0_{As} and Mn levels to depend on the Mn-V^0_{As} separation. Figures 3(b)–3(f) show that for separations larger than $\approx$1.4 nm the lowest of the two (doubly degenerate) V^0_{As} levels is lower than the second Mn level (the one just below the Mn "acceptor"). In an independent electron approximation, occupation of the energy levels of the two separate defects, shown in Fig. 3(a), would therefore be modified by having the V^0_{As} level doubly occupied and the Mn level empty. This change in occupation would therefore make the V_{As} negatively charged and the Mn acceptor doubly charged. Clearly, this result cannot be taken literally. In fact, double occupancy by electrons of the lowest of the two V^0_{As} levels is very unfavorable energetically when electron-electron correlations are included, We expect fluctuations in the charge states near the different defects to play a role in the exact many-body ground state. It is quite possible that the mean electron occupations of the two defect energy levels remains close to the one of Fig. 3(a) at all separations, with the possible exception of the shortest distance at $d = 0.7$ nm; see Fig. 3(f).

Figure 4 shows the LDOS of the Mn-acceptor and V^0_{As} states for the levels shown in Figs. 3(c) and 3(f). The left column in Fig. 4 refers to the case when the distance between the Mn and V^0_{As} is 2.75 nm, while the right column is for 0.7 nm. Figures 4(b) and 4(f) are the LDOS of the Mn-acceptor and Figs. 4(c), 4(d), 4(g), and 4(h) are the V^0_{As} states. The position of the Mn impurity and V^0_{As} on the (110) surface for each column is shown on top of the column [see Figs. 4(a) and 4(e)]. The LDOSs on the left column are similar to the LDOSs of the Mn and the V^0_{As} in the absence of the other defect, due to the large distance between them. When the vacancy is at $d = 0.7$ nm from the Mn (right column), the symmetry of both the Mn-acceptor and the V^0_{As} lowest state (which is closest in energy to the Mn levels) is significantly modified. Let us now consider the effect of V^+_{As} on the Mn acceptor on the GaAs (110) surface. In Fig. 5 we plot the electronic structure for this system inside the GaAs energy gap. Figure 5(a) shows the energy levels of the Mn-impurity and the V^+_{As} calculated separately. Again, we use this level structure, which can be viewed as representing the case of a V^+_{As} placed at a very large separation from the Mn impurity, as a reference for the coupled system. Note that since now the As vacancy has a charge of +1, the total electronic counting given by Eq. (4) is decreased by one unit. Figures 5(b)–5(f) show how the energy levels for the Mn-V^+_{As} system change as V^+_{As} is placed closer to the Mn impurity. The V^+_{As} states are pushed up toward the conduction band as in the case of V^0_{As}. Now however, in contrast to the

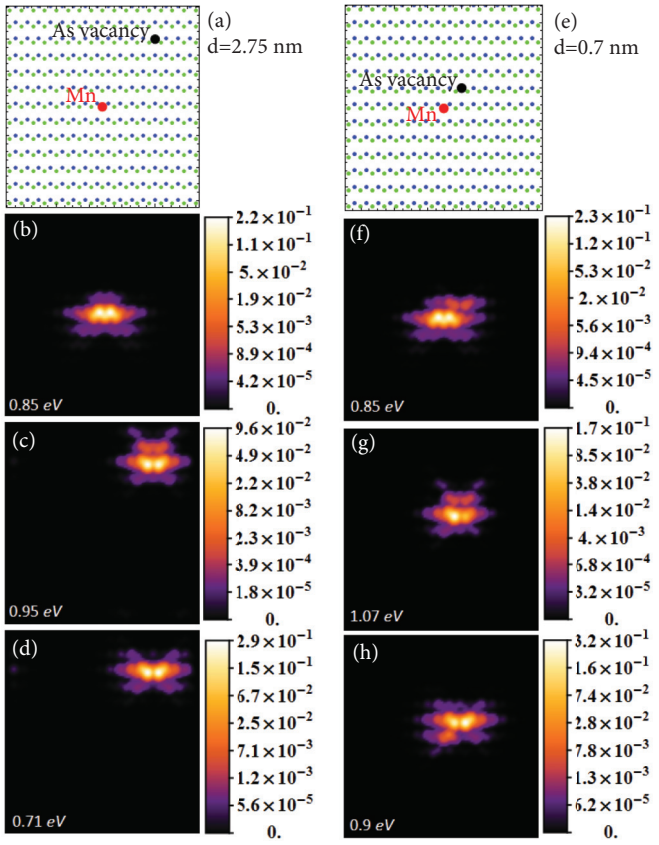

FIG. 4. (Color online) The LDOS of a Mn acceptor and a neutral As vacancy on the GaAs (110) surface for two Mn-V^0_{As} separations. Panels (a) and (e) show the position of the Mn (red circle) and As vacancy (black circle) on the (110) surface. The three pictures below on the left and right refer to these two situations. (b) LDOS of the Mn-acceptor and (c),(d) LDOS of two V^0_{As} states for the level configuration shown in Fig 3(c). Panels (f)–(h) are similar to (b)–(d) for the configuration shown in Fig. 3(f). The LDOS is plotted for one of the two V^0_{As} states belonging to each degenerate level.

V^0_{As} case and in agreement with experiment [5], the energy of the Mn-acceptor state also moves toward the valance band.

Let us look at this result first from the experimental point of view. We know that the bands in a semiconductor bend in the presence of nearby metallic gates, such as the metallic tip of a STM [47–49]. This phenomenon, known as tip-induced band bending (TIBB), is important for the correct interpretation of STM data, particularly in determining the position of impurity levels occurring inside the gap. In STM experiments the TIBB is "negative"; that is, it causes a downward band bending for all voltages below V_{FB}, the voltage that ensures the flat-band condition, TIBB $= 0$. (In Ref. [5], $V_{FB} = +1.6$ V.) The charged vacancies investigated in Ref. [5] and in the present paper can have a similar effect on the bands of the semiconductor host. In analogy to TIBB, this phenomenon is called vacancy-induced band bending (VIBB). VIBB from a positively charged As vacancy is expected to induce a further downward band bending, in addition to the one coming from the TIBB at "negative" voltages. In a rigid band-bending model, where the impurity levels follow rigidly the shift of the host bands, a downward band-bending of the valence band (caused by a combination of TIBB and VIBB) should result in a shift of the acceptor resonant structure, measured in the differential conductance spectra vs the applied STM bias voltage. In particular, this model would predict that the Mn-acceptor resonance should shift toward higher voltages as V^+_{As} is moved closer to the Mn [5]. This would lead to an apparent increase of the acceptor binding energy. The careful experimental results of Ref. [5] find the opposite: The Mn-acceptor binding energy is insensitive to varying TIBB conditions, indicating that the surface-layer Mn levels are detached from the GaAs valence band. Furthermore, the Mn-acceptor binding energy, extracted from the resonances in the differential conductance taken on the Mn, decreases when V^+_{As} is brought closer to the impurity. By ruling out a rigid band bending as the main influence of V^+_{As} on the Mn acceptor, the authors suggested that the decrease in the binding energy of the Mn acceptor is the result of the direct Coulomb repulsion between the V^+_{As} and the Mn hole [50]. In agreement with their experiment, the $(+1)$-charged As vacancy in our calculations, acting as a positive point charge, repels and delocalizes the charged hole bound to the Mn, causing a decrease of its binding energy. The effect makes it possible to locally manipulate the electronic properties of Mn dopants in GaAs by means of an electric field produced by a nearby V^+_{As}.

Figure 6 shows the LDOS for the midgap states of the Mn-impurity–V^+_{As} complex, for the same two defect separations, $d = 2.75$ (left column) and $d = 0.7$ nm (right column), already considered in Fig. 4 for the case of the Mn-impurity–V^0_{As} complex. The states in this picture correspond to the energy levels shown in Figs. 5(c) and 5(f). The two top panels (a) and (b) are the LDOSs for the Mn-acceptor state [that is, the highest unoccupied Mn level in Figs. 5(c) and 5(f)]. A careful analysis of these LDOSs reveals that the Mn-acceptor wave function becomes less localized around Mn impurity as the positive As vacancy is brought closer to the Mn. For example, for $=$ 2.75 nm 23% of the acceptor spectral weight resides on the Mn. This value decreases to only 10% when the separation decreases to $d = 0.7$ nm. This result is consistent with and further confirms the physical mechanism put forward above to account for the decrease of the Mn-acceptor binding energy with decreasing vacancy separation: A positively charged As vacancy repels the Mn acceptor and therefore delocalizes the bound acceptor, leading to a decrease of its binding energy.

Panels (c),(d) and (e),(f) in Fig. 6 refer to the two doubly degenerate V^+_{As} levels. As for the neutral As vacancy, in all cases except for panel (d) the two states belonging to the same doubly degenerate level have very similar LDOS, and therefore only one of them is shown in the figure. The situation in Fig. 6(d) is special. This LDOS is, in fact, the sum of the LDOSs for the two states corresponding to the As energy level located at $\approx$0.65 eV [see Fig. 5(f)]. A careful analysis shows that the energies of these two states are, in fact, split by $\simeq$5 meV. In this case the two wave functions are also quite different, as shown in Fig. 7. One of the two states [Fig. 7(a)] is mainly located on one of the neighboring Ga atoms, while the other [Fig. 7(b)] has a significant contribution also on the As atoms close to the Mn. Clearly, at this close separation the Mn dopant acts like an impurity potential for the As doublet, which is therefore slightly split. In fact, the three top states in Fig. 5(f) (one Mn-impurity and two V^+_{As}) are all quite close in

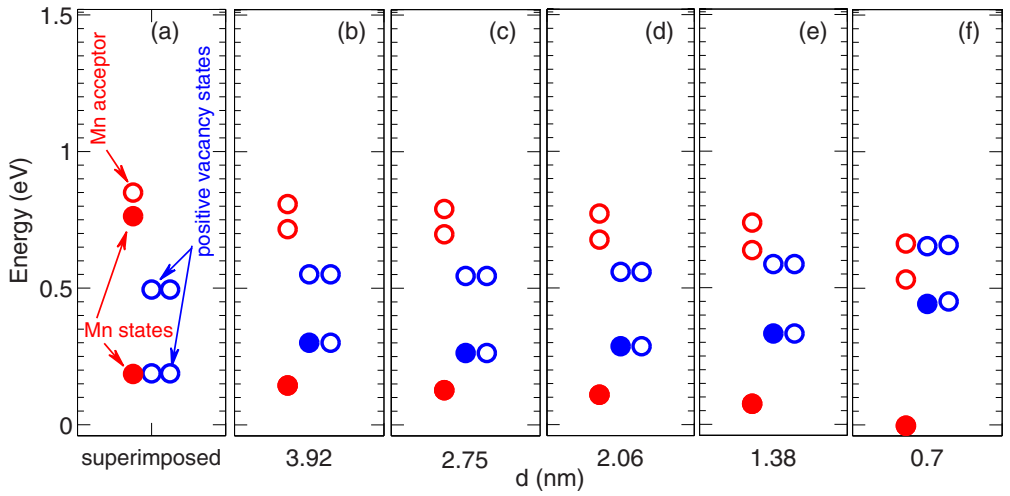

FIG. 5. (Color online) The level structure of a Mn and a positively charged As vacancy on a (110) GaAs surface for different separations, as in Fig. 3. Blue colors indicate vacancy states and red colors indicate Mn states. Solid and open circles distinguish states that are occupied and empty in an independent electron approximation.

energy, and their corresponding wave functions are strongly hybridized. Note that the combined LDOS of these two V^{+}_{As} states resembles quite closely the LDOS of the Mn acceptor.

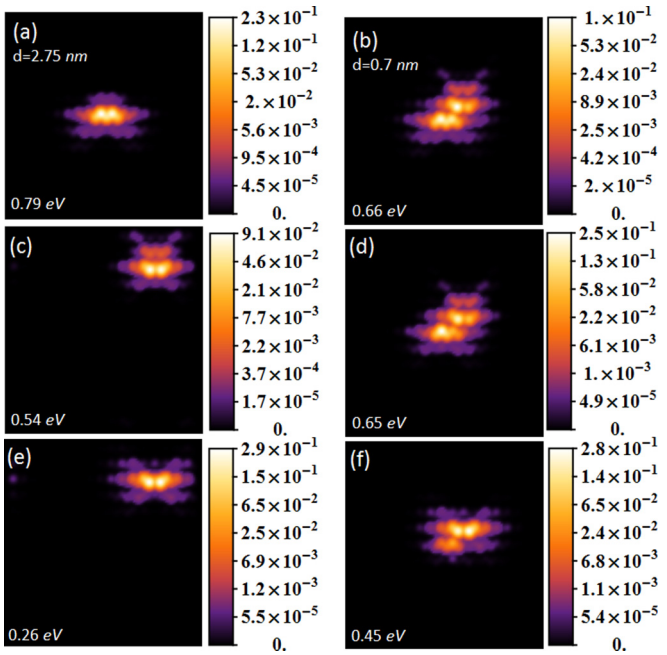

FIG. 6. (Color online) LDOS of the Mn-acceptor state and a V^{+}_{As} state on the GaAs (110) surface for two Mn-V^{+}_{As} separations d. Left column, $d = 2.75$ nm; right column, $d = 0.7$ nm. Positions of the Mn impurity and the As vacancy on the GaAs surface are the same as in Fig. 4. The three LDOSs of the left and right columns correspond to the energy level configurations given in Figs. 5(c) and 5(f), respectively. Panels (a) and (b) represent Mn-acceptor states, while (c)–(e) and (d)–(f) represent V^{+}_{As} states. The two states of each degenerate level of V^{+}_{As} have quite similar LDOSs, except for the LDOS of level at 0.65 eV, shown in panel (d), where we plot the combined LDOSs. The two separate LDOSs for this panel are plotted in Fig 7.

We conclude this section by quantifying the change in the Mn-acceptor binding energy as a function of Mn-impurity–V_{As} separation for the two cases of a neutral and charged vacancy. We define the shift in the Mn-acceptor binding energy caused by the As vacancy, $\Delta\epsilon_{acc}$, as [see Eq. (5)]

$$\Delta\epsilon_{acc}(d) = \epsilon^{ref}_{acc} - \epsilon^{V^{0/+}_{As}}_{acc}(d), \tag{5}$$

where ϵ^{ref}_{acc} is the Mn-acceptor binding energy in the absence of the As vacancy (reference case) and $\epsilon^{V^{0/+}_{As}}_{acc}(d)$ is the Mn-acceptor binding energy when V^{0}_{As}/V^{+}_{As} is at distance d from the Mn impurity. As usual, in all cases we define the Mn-acceptor binding energy as the energy of the highest unoccupied energy level of the Mn impurity in the GaAs energy gap [51]. Note that a positive value of $\Delta\epsilon_{acc}$ corresponds to a decrease in binding energy.

In Fig. 8 we plot $\Delta\epsilon_{acc}(d)$ vs d for both the Mn-impurity–V^{0}_{As} and Mn-impurity–V^{+}_{As} system. This figure summarizes our numerical results for these two cases. V^{0}_{As} does not alter the Mn-acceptor binding energy even at the shortest impurity-vacancy separations (red asterisks in the figure). In contrast, the local electric field generated by V^{+}_{As} has the effect of decreasing $\epsilon^{V^{+}_{As}}_{acc}$, as the As vacancy is brought closer to Mn.

As shown in Fig. 8, the decrease in the Mn-acceptor binding energy with respect to the reference value is 0.11 eV at a separation $d = 1.38$ nm, which matches reasonably well to the experimental value of ≈0.16 eV measured at a separation

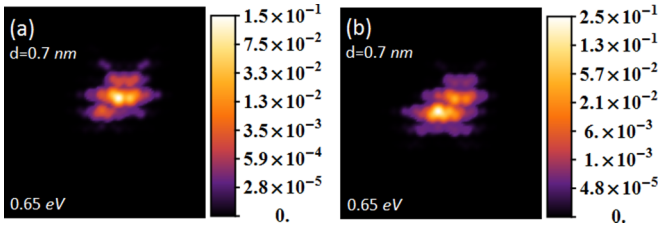

FIG. 7. (Color online) The energy-resolved LDOS for two states of a positively charged As vacancy at 0.65 eV in Fig. 5(f).

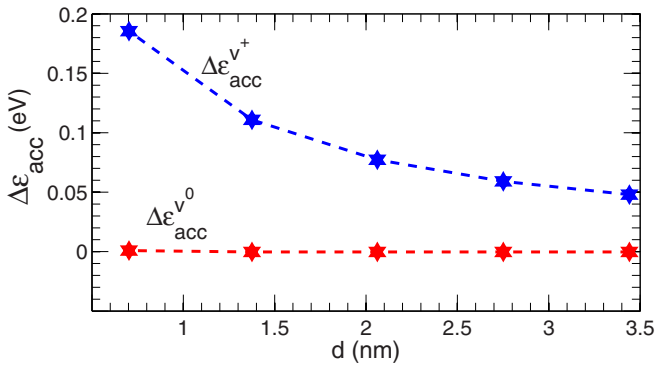

FIG. 8. (Color online) Change in the binding energy of the Mn acceptor caused by a neutral and positive As vacancy [Eq. (5)]. Blue and red asterisks represent the change caused by a positively charged and a neutral As vacancy, respectively.

$d = 1.42$ nm [5]. At a separation $d = 0.7$ nm the calculated acceptor binding energy drops further down by 0.19 eV. There is at present no experimental value at this close separation to compare with.

C. Pairs of ferromagnetically coupled Mn impurities with nearby As vacancies

We now discuss the influence of V_{As}^0 and V_{As}^+ on a pair of ferromagnetically coupled Mn impurities on the (110) surface of GaAs.

In all our calculations we keep the distance between the two Mn impurities fixed, and we vary the distance between the Mn pair and the As vacancy. Specifically, the two Mn dopants are chosen to substitute two nearest-neighbor Ga atoms along the ⟨110⟩ symmetry direction on the (110) surface. Their separation is 0.4 nm. At this distance the exchange-coupling strength between their spins is maximum [27].

Figure 9 shows the energy level structure of a V_{As}^0 and a pair of ferromagnetically coupled Mn impurities inside the GaAs gap. As a reference, in Fig. 9(a) we superimposed the level structure of a V_{As}^0 as well as the topmost six levels of a pair of Mn impurities inside the GaAs gap, calculated separately. For a pair of Mn impurities the two topmost levels of these six levels occurring in the GaAs gap are unoccupied. They are the two acceptor levels introduced by the two Mn impurities, located at 1.34 and 1.67 eV, respectively [52]. The energies of the two acceptor levels are split by a few hundreds of meV only when the spins of the two Mn are coupled ferromagnetically, which is usually the configuration of lowest energy [3,27,34]. In contrast, as shown in Fig. 9(a), if the Mn pair is coupled antiferromagnetically, there is no energy splitting between the two unoccupied acceptors: The topmost unoccupied level is doubly degenerate. Therefore, the splitting between acceptors for a ferromagnetically coupled pair is somewhat related to the ferromagnetic exchange coupling between them [3,27,34]. Since these splittings can be directly probed in STM experiments, it is possible to probe the exchange coupling through tunneling spectroscopy via the acceptor states. Furthermore, since the acceptor energy levels can be electrically manipulated by nearby defects such as As vacancies, the exchange coupling can be indirectly modified by the presence of these extra defects. In Figs. 9(b)–9(f) one can see how the energy levels and in particular how the splitting between the Mn acceptors is modified by the presence of a V_{As}^0 placed at successively shorter separations from the Mn pair. As for the case of an individual Mn, we find that the V_{As}^0 levels are typically pushed up in energy toward the conduction band when approaching the Mn. However, the levels associated with the Mn impurity are hardly modified; in particular, the acceptor splitting remains constant with the exception of the shortest separation $d = 0.7$ nm, where it decreases slightly. As shown in the figure, the electron occupancy of both V_{As}^0 levels and some of the lower Mn levels change as the V_{As}^0 is brought closer to the Mn pair. As mentioned in Sec. III B, some of these results might be affected by on-site electron correlations not included in our model. Note, however, that the acceptor states remain unoccupied at all separations that we considered. It is important to point out that the acceptor splitting is nonzero only for a ferromagnetically coupled Mn pair even in the presence

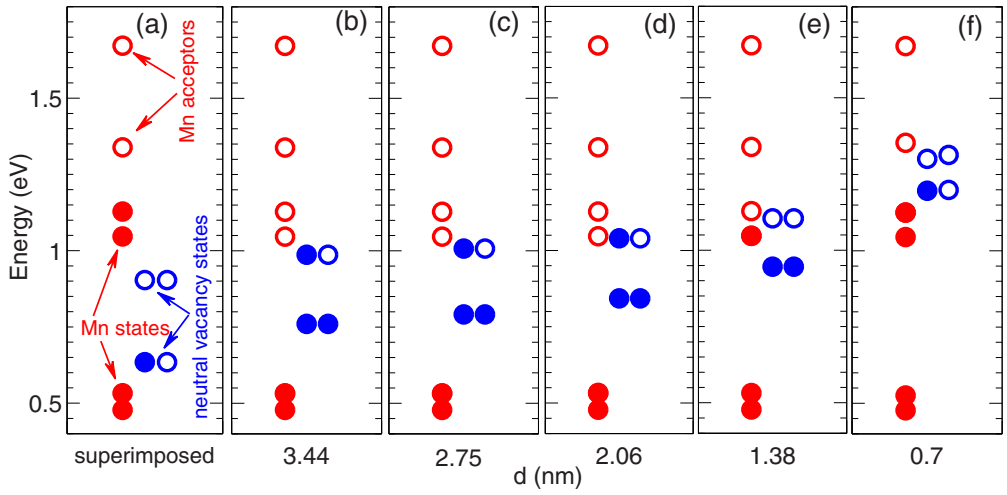

FIG. 9. (Color online) The level structure of a pair of ferromagnetically coupled Mn impurities and a neutral As vacancy on the GaAs (110) surface for different separations; see the caption of Fig. 3. Blue color indicates vacancy states and red color Mn states. Solid and open circles are occupied and empty states, respectively.

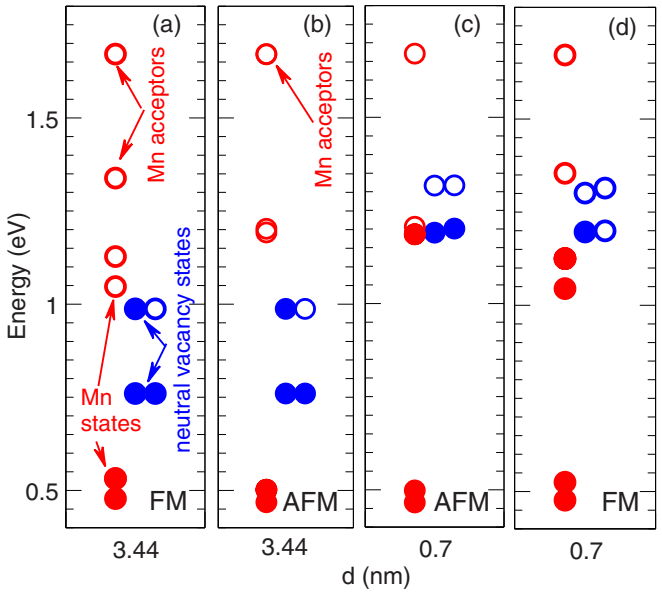

FIG. 10. (Color online) The level structure of a pair of Mn impurities and a neutral As vacancy on the GaAs (110) surface for two different separations; see the caption of Fig. 3. (a),(d) Pair of Mn are ferromagnetically (FM) coupled; (b),(c) pair of Mn are antiferromagnetically (AFM) coupled. Blue color indicates vacancy states and red color Mn states. Solid and open circles are occupied and empty states, respectively. The topmost Mn-acceptor level for the AFM case is doubly degenerate.

of the V^0_{As}. This can be clearly seen in Fig. 10, showing the energy levels at two separations for both a ferromagnetically (FM) coupled Mn pair as well as for an antiferromagnetically (AFM) coupled one. In the second case, the acceptor splitting is identically zero; the topmost level (located at 1.67 eV) is always doubly degenerate.

For the case of a positively charged As vacancy, the picture unfolds in quite a different way. The effect of a V^+_{As} on a pair of Mn dopants at different separations is plotted in Fig. 11. In Fig. 11(a) we plot the superimposed electronic level structure inside the GaAs gap for a V^+_{As} and a Mn pair calculated separately and use it as before as a reference, effectively representing the two defects placed at very large separation. Figures 11(b)–11(f) show the evolution of the electronic structure for the coupled Mn-pair–V^+_{As} system when the two defects approach each other. We find that the two doubly degenerate levels of the V^+_{As} move progressively toward the conduction band under the effect of the Mn-pair potential. In contrast, five of the six levels of the Mn pair, including the lowest of the two Mn-acceptor levels [the lowest unoccupied level in Fig. 11(a)] are pushed down towards the valence band. The mechanism responsible for these two combined effects is essentially the same as for the case of one individual Mn impurity in the presence of a V^+_{As}. The repulsive potential coming from the Mn ion pushes away electrons and tends to localize holes closer to the Mn core, increasing the energy of the As levels. Similarly, the attractive potential (for the electrons) coming from the V^+_{As} tend to delocalize the Mn acceptor, thereby pushing their energies toward the valance band. Interestingly, the top Mn acceptor (the highest unoccupied Mn level in all panels of Fig. 11) is the only one that defies this rule: Way up in energy and close to the conduction band edge, this level is hardly affected by the presence of V^+_{As}, even at the shortest distances. This has important implications on the relative splitting of the two Mn-acceptor levels, discussed below.

The energy level occupancy for the energy levels of the coupled system remains the same at all separations. The main difference with respect to the reference state [Fig. 11(a)] is the double occupancy of the lowest V^+_{As} level (which is empty for an isolated V^+_{As}) at the expenses of the two Mn levels (occupied for the isolated pair) located around 1 eV. As mentioned before, it is likely that these results are strongly altered by on-site electronic correlations which suppress the double occupancy probability. In any case, our numerical calculations show that the two Mn acceptors (i.e., the two topmost levels of the Mn pair) are always unoccupied, as for the case of an isolated Mn pair, regardless of the position of the As vacancy. This result,

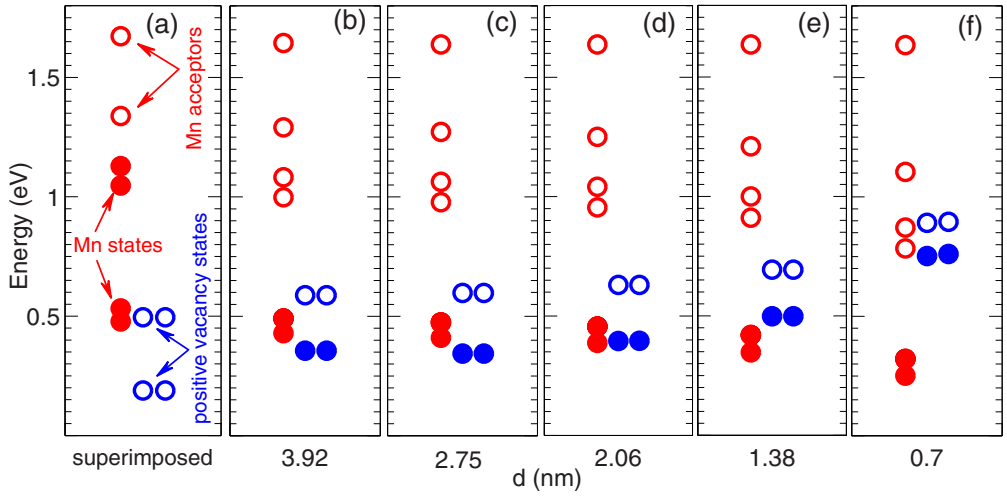

FIG. 11. (Color online) The level structure of a pair of FM coupled Mn impurities and a positively charged As vacancy on the GaAs (110) surface for different defect separations; see the caption of Fig. 3. Blue color indicates vacancy states and red color Mn states. Solid and open circles indicate occupied and empty states levels in an independent-electron approximation.

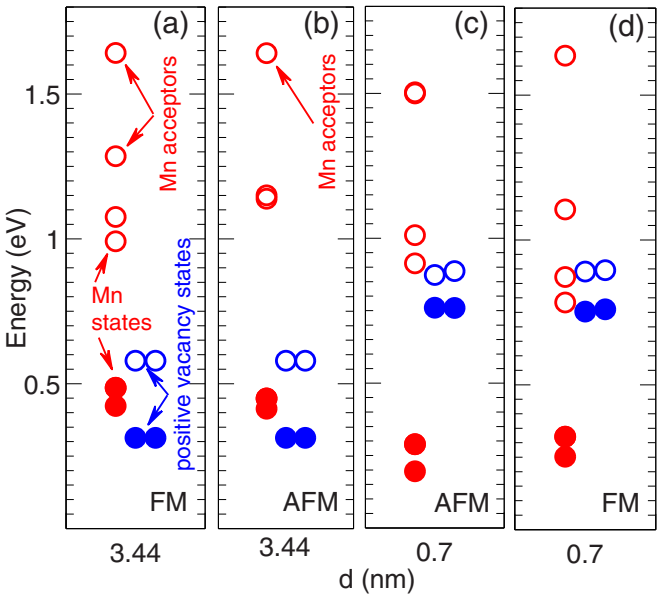

FIG. 12. (Color online) The level structure of a pair of Mn impurities and a positively charged As vacancy on the GaAs (110) surface for two different defect separations. See caption of Fig. 3. (a),(d) The spins of the two Mn atoms are FM coupled. (b),(c) The spins of the two Mn atoms are AFM coupled. Blue color indicates vacancy states and red color Mn states. Solid and open circles are occupied and empty states, respectively. The topmost Mn-acceptor level for the AFM case is doubly degenerate.

involving levels high up in energy and separated from the other impurity levels, should be rather robust against on-site correlations. Furthermore, as Fig. 12 shows, the energies of these two levels are split when the spins of the two Mn atoms are aligned FM, but essentially degenerate for AFM coupling. Therefore, we reach the important conclusion that the splitting of the two Mn-acceptor energy levels, $\epsilon_{\mathrm{acc}_1}$ and $\epsilon_{\mathrm{acc}_2}$,

$$\Delta\epsilon_i = \epsilon_{\mathrm{acc}_1} - \epsilon_{\mathrm{acc}_2}, \tag{6}$$

is an indicator of the FM state of the Mn pair even in the presence of V^+_{As}, as it is in the presence of V^0_{As} as well as for the isolated pair. In Fig. 13 we plot $\Delta\epsilon_i(d)$ as a function of the Mn-pair–V_{As} separation, d, for the cases of a neutral (red asterisks) and a charged As vacancy (blue asterisks). We can see that V^0_{As} has no effect on $\Delta\epsilon_i(d)$, except for the shortest separation $d = 0.7$ nm, where the splitting decreases by merely ≈50 meV. On the other hand, our calculations show that V^+_{As} significantly modifies $\Delta\epsilon_i(d)$, as V^+_{As} is brought closer to the Mn pair and $\Delta\epsilon_i(d)$, which is equal to 0.36 eV without any vacancy nearby, increases to 0.53 eV at a separation of 0.7 nm. This figure summarizes our findings on how an As vacancy affects the electronic and magnetic properties of a Mn pair in GaAs.

Since $\Delta\epsilon_i$ is an indication of the strength of the exchange coupling between two Mn ions, these theoretical predictions open up the possibility of manipulating the exchange splitting by the electrostatic field of nearby As vacancies.

In the last part of this section, we discuss the calculated LDOS for a Mn pair in the presence of an As vacancy, which can provide useful information for ongoing STM experiments. As an example, we consider the case of V^+_{As}. In Fig. 14 we

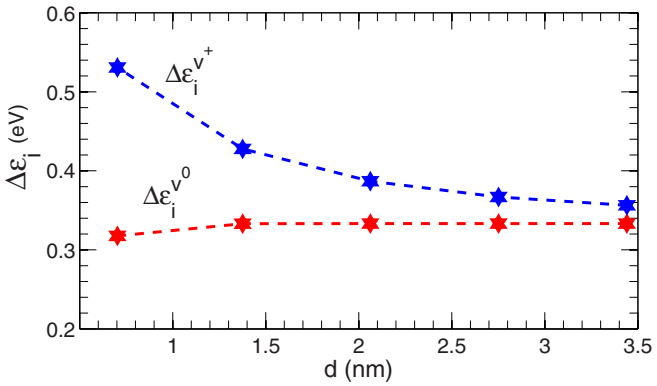

FIG. 13. (Color online) Change in the energy splitting between the two acceptors levels of a Mn pair [Eq. (6)] caused by a neutral and a positively charged vacancy placed at a distance d from the Mn pair. Red and blue asterisks represent the case of a neutral and a charged As vacancy, respectively.

display the LDOS for the defects states inside the GaAs gap for two defect separations, $d = 2.75$ nm (left column) and $d = 0.7$ nm (right column). The electronic energy levels for these two cases were given in Figs. 11(c) and 11(f), respectively. In Figs. 14(a) and 14(b) we show the positions of the Mn-pair (red circles) and V^+_{As} (black circle) on the GaAs (110) surface for the two defect separations. Figures 14(c) and 14(d) and Figs. 14(e) and 14(f) show the LDOS of the highest and lowest acceptors, respectively. The LDOS of the highest acceptor shows a quite delocalized state, since, as mentioned above, for the present choice of the TB parameters, this level, located at 1.67 eV, has merged with the conduction band. By tuning the value of V_{corr} in Eq. (2), it is possible to bring this level back inside the top of the band gap, in the position where it is seen experimentally (≈1.03 eV). In this case, the corresponding wave function not only is strongly localized around the Mn, but it also has a bonding character, with maximum spectral weight on the As atom between the Mn atoms [3,27]. The bonding character for the highest acceptor can be seen, albeit very slightly, in Figs. 14(c) and 14(d); although the wave function is delocalized, it has a clear maximum on the As between the Mn atoms of the pair.

For the lowest acceptor state, the picture is different. As shown in Fig. 14(e), when the As vacancy is far away, the acceptor state has an antibonding character [27], with ≈52% of its total spectral weight equally distributed on each of the two Mn atoms, and a small contribution on the As in between [27]. When the As vacancy is at 0.7 nm from the Mn-pair [Fig. 14(f)], only ≈16% of the acceptor spectral weight is located on the Mn atom closest to the As vacancy, and ≈36% is on the furthest Mn. The rest of the acceptor wave function is pushed further away from the vacancy. This confirms the repulsion between the V^+_{As} and the hole bound to Mn. Clearly, the Mn-acceptor states hybridize very little with the V^+_{As} states, even at the shortest separation, which is consistent with the level structure shown in Fig. 11(f). The V^+_{As} states, however, behave differently. As shown in Figs. 14(h) and 14(j) the combined LDOS of the two V^+_{As} levels is strongly modified when the defect separation is only $d = 0.7$ nm. A careful analysis of this case shows that the two V^+_{As} strongly hybridize

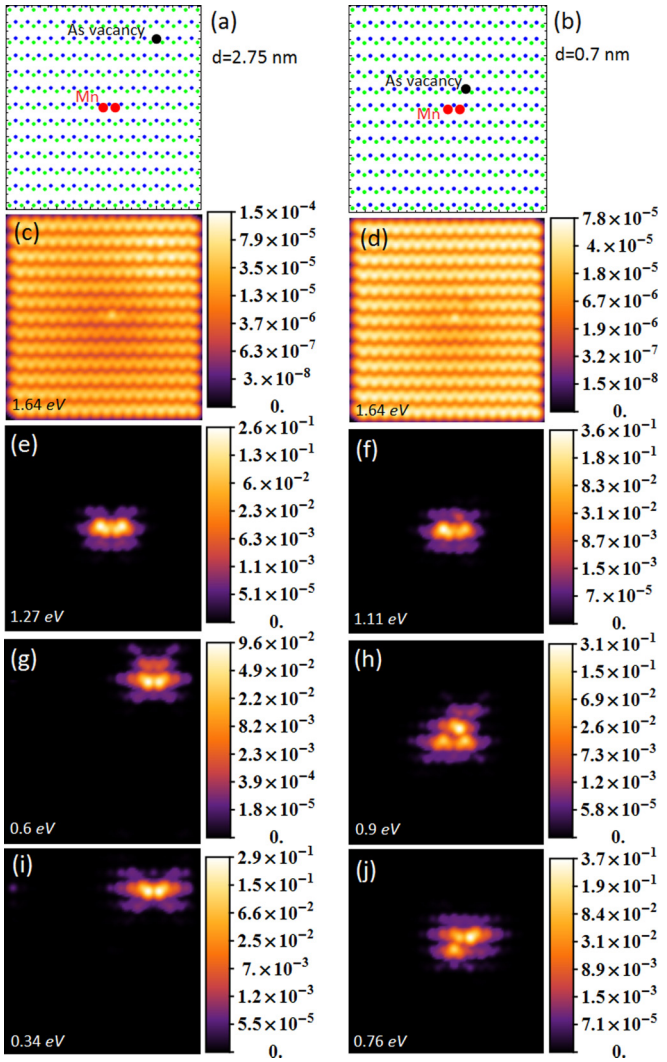

FIG. 14. (Color online) LDOS of the defect states inside the GaAs energy gap for a system composed of a FM coupled Mn pair in the presence of a positively charged As vacancy on the GaAs (110) surface. Two defect separations are considered: left column, $d = 2.75$ nm; right column, $d = 0.7$ nm. The energy level structure inside the gap for these two defect configurations is shown in Figs. 11(c) and 11(f), respectively. (a),(b) Position of the two defects on the GaAs (110) surface for left and right columns, respectively. (c),(d) LDOS of Mn-pair acceptors at 1.64 eV. (e),(f) LDOS of Mn-pair acceptors at 1.27 and 1.11 eV. (g),(i) LDOS of the two V^{+}_{As} energy levels in Fig. 11(c). Each level is doubly degenerate and two corresponding states have similar LDOS. (h),(j) LDOS of the two V^{+}_{As} energy levels in Fig. 11(f). Each level is a quasi doubly degenerate level (they are both slightly split by a few meV); (h) and (j) represent the combined LDOS of the two corresponding states. The energy-resolved LDOSs for these two pairs of states are plotted in Fig. 15.

with other Mn-pair states (not the acceptor) that are close in energy, according to Fig. 11(f). Because of this coupling with the states of the Mn-pair, the two V^{+}_{As} levels, which are essentially doubly degenerate at $d = 2.75$ nm, are slightly split at the shortest separation (4 meV for the level at 0.9 eV and 9 meV for the level at 0.75 eV). The energy-resolved LDOS of two corresponding states (originating from the same level)

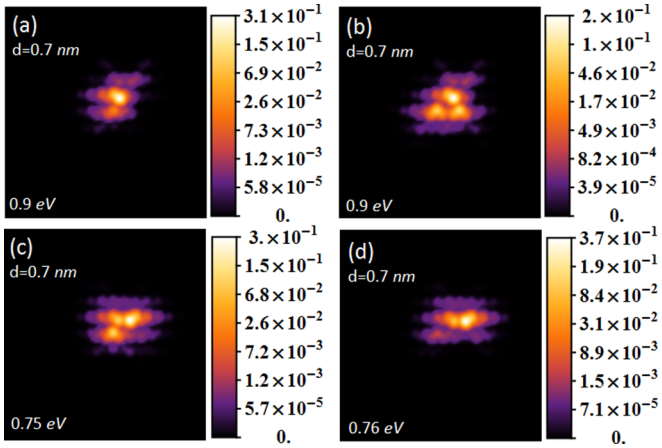

FIG. 15. (Color online) Energy-resolved LDOS for the two pairs of states corresponding to the two V^{+}_{As} quasidegenerate energy levels at 0.9 and 0.76 eV in Fig. 11(f). Both levels are, in fact, slightly split, by 4 and 9 meV, respectively.

now look very different, as shown in Fig. 15, as a result of the different hybridization with the Mn states. This is the precisely same phenomenon that we encountered above when studying As vacancies in the vicinity of *individual* Mn impurities.

It is important to point out that the modification of the V^{+}_{As} states due to the hybridization with the Mn states occurring at very short separations has nothing to do with the shift of the Mn-acceptor levels caused by the Coulomb potential of the charged As vacancy. Indeed, similar hybridization-induced deformations of the LDOS occur also in the presence of neutral As vacancies, where the Mn-acceptor energies are left essentially unchanged. Nevertheless, the change in the V_{As} state wave functions caused by nearby Mn impurities (individual or pairs) should be detectable in STM experiments.

IV. CONCLUSIONS

Motivated by STM experiments [5], we have studied theoretically the effect of neutral and positively charged As vacancies on the electronic and magnetic properties of the acceptor state of Mn impurities on the GaAs (110) surface. For the calculations we used an atomistic TB model in the mean-field approximation for large finite clusters containing up to 8840 atoms, allowing us to address (110) surface areas on the order of 6.6×7.1 nm^2 and Mn-As separations more than 4 nm. The model has been quite successful recently in describing the physics of individual and pairs of substitutional Mn atoms on the (110) surface [26,27]. For individual isolated As vacancies, both neutral and positively charged, the model is able to reproduce the electronic structure, explained earlier using *ab initio* methods [9,15,17], characterized by two in-gap doubly degenerate levels, which are both empty for V^{+}_{As}, while half filled and empty in the case of V^{0}_{As}. These results are remarkable, since they are obtained within an independent electron approximation where both types of As vacancies are modeled by effective single-particle potentials, without requiring self-consistency in the charge distribution.

The focus of the paper has been the analysis of the Mn-acceptor binding energy, as a function of the separation between the Mn impurity and V_{As}. The model correctly

reproduces the experimental findings that the Mn-acceptor binding energy is unaffected by the presence of nearby neutral vacancies, and that the binding energy decreases significantly when a charged As is brought closer to the Mn. The numerical results supports the hypothesis put forward in Ref. [5] that the shift in the resonant spectra of Mn in STM experiments is not a trivial As-vacancy-induced band-bending effect, but rather a genuine modification of the Mn-acceptor level due to the direct Coulomb repulsion of the positively charged Mn-acceptor hole by V_{As}^{+}. Indeed, our calculations of the acceptor LDOS show that a decrease of the Mn-acceptor binding energy by a nearby V_{As}^{+} is accompanied by increased delocalization of the acceptor-hole wave function. We stress that in order to investigate Mn-impurity–V_{As} separations close to the ones studied experimentally (≈4 nm), large supercells are needed. This gives our TB model an advantage over *ab initio* methods based on DFT, which typically have much smaller maximum supercell sizes.

The calculations also show that the electronic energy level structure of the coupled Mn-impurity–V_{As} system is considerably more complex than the electronic structure of isolated individual defects and less suitable for independent-electron approximation treatments. This limitation applies equally well to our TB approach and to approaches which involve solutions of the Kohn-Sham equations of density functional theory. In particular, our model predicts the possibility of electron charge switching between the levels of the two defects as a function of their separation, leading to a modification of the in-gap resonant spectra in STM experiments, and the appearance of new transport channels. We emphasize that these results are obtained within a non-self-consistent one-particle theory, which neglects Coulomb correlations. Such correlations are important in determining the mean level occupancy, and likely to lead to correlation-induced fluctuating valences on both defects. The coupling of the Mn-impurity and V_{As} states inside the gap gives rise to strongly hybridized wave functions at short separations, and the LDOS at the position of each defect is deformed by the presence of the other. These effects should be visible in STM experiments when the defect separation is smaller than 1 nm.

In the second part of the paper we have investigated the effect of V_{As} on pairs of FM coupled Mn atoms. Here our calculations predict that the energies of the two unoccupied Mn-acceptor levels, which are split if the spins of the two Mn atoms are parallel, move further apart when a V_{As}^{+} approaches the Mn pair. We have shown that the mechanism behind this effect is essentially related to the reduction of the Mn-acceptor binding energy present in the case of individual Mn impurities. Consistently with this result, a neutral V_{As} does not have any effect on the acceptor splitting. Previous experimental [3] and theoretical work [3,27,34] has shown that the acceptor splitting of the Mn pair, which appears as a double in-gap resonance in STM measurements, is an indication of the strength of the exchange interaction between the two magnetic atoms. The results presented here suggest that it might be possible to control and manipulate the Mn exchange coupling in GaAs with local electric fields at the atomic scale, by means of As vacancies positioned nearby with atomic precision. Since the charge state of the As vacancy can be reversibly swapped between neutral and charged by the STM tip, this effect could be used to rapidly turn on and off locally the exchange coupling between the two magnetic atoms.

Note that in this paper we have only considered the case of two Mn atoms placed at the shortest separation from each other. This choice maximizes the acceptor splitting and the exchange interaction. It is known that the exchange interaction on the (110) surface is strongly anisotropic with respect to the orientation along the crystal axis [3,27,34]. A careful choice of both the Mn-pair orientation and the As vacancy location could result in situations where the local exchange coupling can be rapidly switched in real time between two quite different values.

ACKNOWLEDGMENTS

This work was supported by the Faculty of Technology at Linnaeus University, by the Swedish Research Council under Grant No. 621-2010-3761, by the NordForsk research network Grant No. 080134 "Nanospintronics: Theory and Simulations," by the Welch Foundation under Grant No. TBF1473, and by the DOE Division of Materials Sciences and Engineering under Grant No. DE- FG03-02ER45958. Computational resources have been provided by the Center for Scientific and Technical Computing LUNARC at Lund University. We are very grateful to J. A. Gupta for useful discussions and illuminating explanations of the experimental results.

[1] A. M. Yakunin, A. Y. Silov, P. M. Koenraad, J. H. Wolter, W. Van Roy, J. De Boeck, J.-M. Tang, and M. E. Flatté, Phys. Rev. Lett. **92**, 216806 (2004).
[2] A. M. Yakunin, A. Y. Silov, P. M. Koenraad, J.-M. Tang, M. E. Flatté, W. Van Roy, J. De Boeck, and J. H. Wolter, Phys. Rev. Lett. **95**, 256402 (2005).
[3] D. Kitchen, A. Richardella, J.-M. Tang, M. E. Flatté, and A. Yazdani, Nature (London) **442**, 436 (2006).
[4] D. Kitchen, A. Richardella, P. Roushan, J.-M. Tang, M. E. Flatté, and A. Yazdani, J. Appl. Phys. **101**, 09G515 (2007).
[5] D. H. Lee and J. A. Gupta, Science **330**, 1807 (2010).
[6] S. B. Zhang and A. Zunger, Phys. Rev. Lett. **77**, 119 (1996).
[7] J. E. Northrup and S. B. Zhang, Phys. Rev. B **50**, 4962 (1994).
[8] S. B. Zhang and J. E. Northrup, Phys. Rev. Lett. **67**, 2339 (1991).
[9] H. Kim and J. R. Chelikowsky, Phys. Rev. Lett. **77**, 1063 (1996).
[10] H. Seong and L. J. Lewis, Phys. Rev. B **52**, 5675 (1995).
[11] M. S. Daw and D. L. Smith, Phys. Rev. B **20**, 5150 (1979).
[12] G. Lengel, R. Wilkins, G. Brown, and M. Weimer, J. Vac. Sci. Technol., B: Microelectron. Process. Phenom. **11**, 1472 (1993).
[13] S. Aloni, I. Nevo, and G. Haase, J. Chem. Phys. **115**, 1875 (2001).
[14] G. Lengel, R. Wilkins, G. Brown, M. Weimer, J. Gryko, and R. E. Allen, Phys. Rev. Lett. **72**, 836 (1994).
[15] H. Kim and J. R. Chelikowsky, Surf. Sci. **409**, 435 (1998).

[16] J.-Y. Yi, J. S. Ha, S.-J. Park, and E.-H. Lee, Phys. Rev. B **51**, 11198 (1995).
[17] K.-J. Chao, A. R. Smith, and C.-K. Shih, Phys. Rev. B **53**, 6935 (1996).
[18] Y. Zhao, P. Mahadevan, and A. Zunger, Apl. Phys. Lett. **19**, 3753 (2004).
[19] P. Mahadevan, A. Zunger, and D. D. Sarma, Phys. Rev. Lett. **93**, 177201 (2004).
[20] A. Mikkelsen, B. Sanyal, J. Sadowski, L. Ouattara, J. Kanski, S. Mirbt, O. Eriksson, and E. Lundgren, Phys. Rev. B **70**, 085411 (2004).
[21] M. F. Islam and C. M. Canali, Phys. Rev. B **85**, 155306 (2012).
[22] J.-M. Tang and M. E. Flatté, Phys. Rev. Lett. **92**, 047201 (2004).
[23] J.-M. Tang and M. E. Flatté, Phys. Rev. B **72**, 161315 (2005).
[24] C. Timm and A. H. MacDonald, Phys. Rev. B **71**, 155206 (2005).
[25] J.-M. Jancu, J.-C. Girard, M. O. Nestoklon, A. Lemaitre, F. Glas, Z. Z. Wang, and P. Voisin, Phys. Rev. Lett. **101**, 196801 (2008).
[26] T. O. Strandberg, C. M. Canali, and A. H. MacDonald, Phys. Rev. B **80**, 024425 (2009).
[27] T. O. Strandberg, C. M. Canali, and A. H. MacDonald, Phys. Rev. B **81**, 054401 (2010).
[28] T. O. Strandberg, C. M. Canali, and A. H. MacDonald, Phys. Rev. Lett. **106**, 017202 (2011).
[29] J. Mašek, F. Máca, J. Kudrnovský, O. Makarovsky, L. Eaves, R. Campion, K. Edmonds, A. Rushforth, C. Foxon, B. Gallagher *et al.*, Phys. Rev. Lett. **105**, 227202 (2010).
[30] M. Bozkurt, M. R. Mahani, P. Studer, J.-M. Tang, S. R. Schofield, N. J. Curson, M. E. Flatté, A. Y. Silov, C. F. Hirjibehedin, C. M. Canali, and P. M. Koenraad, Phys. Rev. B **88**, 205203 (2013).
[31] A. Richardella, D. Kitchen, and A. Yazdani, Phys. Rev. B **80**, 045318 (2009).
[32] A. Stroppa, X. Duan, M. Peressi, D. Furlanetto, and S. Modesti, Phys. Rev. B **75**, 195335 (2007).
[33] M. R. Mahani, M. F. Islam, A. Pertsova, and C. M. Canali, Phys. Rev. B **89**, 165408 (2014).
[34] J.-M. Tang and M. E. Flatté, Proc. SPIE **7398**, 73980K (2009).
[35] J. C. Slater and G. F. Koster, Phys. Rev. **94**, 1498 (1954).
[36] D. A. Papaconstantopoulos and M. J. Mehl, J. Phys.: Condens. Matter **15**, R413 (2003).
[37] D. J. Chadi, Phys. Rev. Lett. **41**, 1062 (1978).
[38] D. J. Chadi, Phys. Rev. B **19**, 2074 (1979).
[39] H. Ohno, Science **281**, 951 (1998).
[40] D. J. Chadi, Phys. Rev. B **16**, 790 (1977).
[41] J. K. Garleff, A. P. Wijnheijmer, A. Y. Silov, J. van Bree, W. Van Roy, J.-M. Tang, M. E. Flatté, and P. M. Koenraad, Phys. Rev. B **82**, 035303 (2010).
[42] W. Schairer and M. Schmidt, Phys. Rev. B **10**, 2501 (1974).
[43] T. Lee and W. W. Anderson, Solid State Commun. **2**, 265 (1964).
[44] R. A. Chapman and W. G. Hutchinson, Phys. Rev. Lett. **18**, 443 (1967).
[45] M. Linnarsson, E. Janzen, B. Monemar, M. Kleverman, and A. Thilderkvist, Phys. Rev. B **55**, 6938 (1997).
[46] M. R. Mahani, A. Pertsova, and C. M. Canali, J. Phys.: Condens. Matter **26**, 394006 (2014).
[47] R. M. Feenstra and J. A. Stroscio, J. Vac. Sci. Technol., B: Microelectron. Process. Phenom. **5**, 923 (1987).
[48] R. M. Feenstra, J. Vac. Sci. Technol., B: Microelectron. Process. Phenom. **21**, 2080 (2003).
[49] N. Ishida, K. Sueoka, and R. M. Feenstra, Phys. Rev. B **80**, 075320 (2009).
[50] It is interesting to point out that in Ref. [5] in-gap resonances of STM spectra taken on subsurfaces Zn acceptors shift toward *higher* voltage as V_{As}^{+} is moved closer. A numerical simulation shows that in this case the rigid band-bending model reproduces perfectly the influence of the As vacancy on the acceptor position.
[51] For the case of one Mn on the (110) surface, the Mn acceptor defined in this way is always a midgap state. For a Mn pair discussed in the next section, we see that one of the two acceptors ends in the conduction band.
[52] Note that for the choice of the parameters presently used in the TB Hamiltonian, the topmost Mn-acceptor level with energy equal to 1.67 eV, is, in fact, merging with the conduction band. Experimentally, this level is found to be at 1.4 eV, that is, still inside the band gap but quite close to the conduction band edge (located at 1.52 eV). Its position in our calculations can be tuned to the experimental value by choosing an appropriate value of V_{corr} [27].